




The RNA-binding protein QKI-7 recruits the poly(A) polymerase GLD-2 for 3' adenylation and selective stabilization of microRNA-122

Received for publication, October 28, 2019, and in revised form, November 15, 2019. Published, Papers in Press, December 1, 2019, DOI 10.1074/jbc.RA119.011617

Hiroaki Hojo[‡], Yuka Yashiro[‡], Yuta Noda[‡],  Koichi Ogami[§], Ryota Yamagishi[§], Shunpei Okada[‡], Shin-ichi Hoshino[§], and  Tsutomu Suzuki^{‡1}

From the [‡]Department of Chemistry and Biotechnology, Graduate School of Engineering, University of Tokyo, 7-3-1 Hongo, Bunkyo-ku, Tokyo 113-8656, Japan and the [§]Department of Biological Chemistry, Graduate School of Pharmaceutical Sciences, Nagoya City University, Nagoya 467-8603, Japan

Edited by Ronald C. Wek

MicroRNA-122 (miR-122) is highly expressed in hepatocytes, where it plays an important role in regulating cholesterol and fatty acid metabolism, and it is also a host factor required for hepatitis C virus replication. miR-122 is selectively stabilized by 3' adenylation mediated by the cytoplasmic poly(A) polymerase GLD-2 (also known as PAPD4 or TENT2). However, it is unclear how GLD-2 specifically stabilizes miR-122. Here, we show that QKI7 KH domain-containing RNA binding (QKI-7), one of three isoforms of the QKI proteins, which are members of the signal transduction and activation of RNA (STAR) family of RNA-binding proteins, is involved in miR-122 stabilization. QKI down-regulation specifically decreased the steady-state level of mature miR-122, but did not affect the pre-miR-122 level. We also found that QKI-7 uses its C-terminal region to interact with GLD-2 and its QUA2 domain to associate with the RNA-induced silencing complex protein Argonaute 2 (Ago2), indicating that the GLD-2–QKI-7 interaction recruits GLD-2 to Ago2. QKI-7 exhibited specific affinity to miR-122 and significantly promoted GLD-2–mediated 3' adenylation of miR-122 *in vitro*. Taken together, our findings indicate that miR-122 binds Ago2–interacting QKI-7, which recruits GLD-2 for 3' adenylation and stabilization of miR-122.

MicroRNAs (miRNAs)² constitute a large family of ~21-nucleotide RNAs that silence specific mRNAs and thereby regulate various biological processes related to development, differ-

entiation, physiology, and pathology. miRNA associates with Argonaute (Ago) and other proteins to form the RNA-induced silencing complex (RISC), which binds to a sequence complementary to the miRNA in the 3'-untranslated region (UTR) of the target mRNA, leading to translational repression, 3' deadenylation, and degradation (1, 2). Expression of most miRNAs is spatiotemporally regulated, and alteration of individual miRNA levels can result in pathological consequences. Accordingly, the steady-state levels of miRNAs are tightly controlled at multiple levels, including miRNA transcription, processing of precursors by Drosha or Dicer, and degradation of mature miRNA (3).

Several mechanisms that regulate miRNA stability and degradation have been elucidated (4, 5). In particular, the 3' termini of miRNAs frequently undergo post-transcriptional uridylation, adenylation, and 2'-O-methylation, and these modifications play major roles in regulating the stability of miRNAs. In mammals, Lin28B binds to the terminal loop of pre-let-7 and recruits TUT4 (also known as ZCCHC11) and TUT7 (also known as ZCCHC6), leading to oligouridylation of pre-let-7 (6–8). This modification prevents pre-let-7 processing by Dicer, resulting in 3'-5' exonucleolytic degradation mediated by Dis3l2 (9). In the absence of Lin28, TUT4 and TUT7 monouridylate a subset of pre-miRNAs at their 3' termini to facilitate dicing for miRNA maturation (10). In plants, the 3' termini of miRNAs and siRNAs are 2'-O-methylated by Hen1 methyltransferase during maturation (11). This terminal methylation prevents 3'-oligouridylation by HESO1 (11–13). Because oligouridylated miRNAs are degraded by 3' exonuclease SDN (14), by preventing oligouridylation the terminal methylation protects the 3' termini of miRNAs and blocks degradation. In mammals and *Drosophila melanogaster*, the 3' termini of piRNAs and siRNAs, rather than miRNAs, are 2'-O-methylated by Hen1 homologs (Pimet and DmHen1) (15–18).

The liver-specific miRNA miR-122, which is highly expressed in hepatocytes and some hepatoma cells, plays an important role in hepatic function by regulating cholesterol and fatty acid metabolism (19, 20). miR-122 is also a host factor required for hepatitis C virus replication (21–23). We reported previously that the steady-state level of miR-122 is determined by the balance between GLD-2 (also referred to as PAPD4 or TENT2) mediated 3' adenylation and PARN-mediated 3' deadenylation and degradation (24, 25). In the livers of GLD-2–null

This work was supported by Grants-in-Aid for Scientific Research on Priority Areas from the Ministry of Education, Culture, Sports, Science, and Technology of Japan (MEXT) and the Japan Society for the Promotion of Science (JSPS) (to T. S.), and the Program on the Innovative Development and the Application of New Drugs for Hepatitis B from the Japan Agency for Medical Research and Development (AMED) (to S.-i. H.). The authors declare that they have no conflicts of interest with the contents of this article.

This article contains Figs. S1 and S2 and Table S1.

¹ To whom correspondence should be addressed. E-mail: ts@chembio.t.u-tokyo.ac.jp.

² The abbreviations used are: miRNA, microRNA; Ago, Argonaute; RISC, RNA-induced silencing complex; HCV, hepatitis C virus; CUGBP1, CUG-binding protein 1; STAR, signal transduction and activation of RNA; NSC, neural stem cell; QRE, QKI response element; KD, knockdown; IP, immunoprecipitated; NT, nucleotidyltransferase; EMSA, electrophoretic mobility shift assay; HA, hemagglutinin; DAPI, 4',6-diamidino-2-phenylindole; GST, glutathione S-transferase; GAPDH, glyceraldehyde-3-phosphate dehydrogenase; WB, Western blot.

mice, 3' adenylation of miR-122 disappears, and the steady-state level of miR-122 is markedly reduced. By contrast, in PARN knockdown cells, miR-122 is 3'-oligoadenylated and its steady-state level is elevated. In primary fibroblasts, GLD-2-mediated 3' adenylation of miR-122 regulates the expression of *CPEB* mRNA, leading to polyadenylation and translation of *p53* mRNA (26, 27). Thus, miR-122 controls cellular senescence via post-transcriptional control of p53.

GLD-2 adenylates several other miRNAs in mammals (28), but this modification does not always contribute to their stability. A recent study demonstrated that the HCV core protein interacts with GLD-2 and inhibits its 3' adenylase activity, thereby destabilizing miR-122 and decreasing HCV RNA abundance (29). Thus, the HCV core protein controls viral replication levels by down-regulating miR-122. Regarding the molecular mechanism underlying selective destabilization of miR-122, we reported that an RNA-binding protein, CUG-binding protein 1 (CUGBP1), specifically binds to miR-122 and recruits PARN, thereby stimulating 3' deadenylation and degradation (25). However, it remains unclear how GLD-2 specifically stabilizes miR-122.

QKI is a conserved multifunctional protein belonging to the STAR (signal transduction and activation of RNA) family of RNA-binding proteins. QKI proteins are involved in various aspects of post-transcriptional regulation of mRNAs, including stability, splicing, and translation (30–33). Dysregulation of QKI is associated with human diseases such as schizophrenia, ataxia, and glioblastoma (31–35). QKI is a major regulator of neural stem cell (NSC) stemness, and deletion of *Qki* in mice promotes NSC self-renewal and inhibits NSC differentiation in suboptimal environments (36). In addition, QKI promotes circular RNA biogenesis during the epithelial-to-mesenchymal transition (37). Three major isoforms, QKI-5, QKI-6, and QKI-7, are produced from the single *QKI* gene by alternative splicing (38). These isoforms all contain the same QUA1, QUA2, and KH domains in the N-terminal region, but their 8–30 C-terminal amino acids differ (39)(see Fig. 2B). QKI-5 contains a nuclear localization signal, and accordingly is predominantly localized in nucleus (30). QKI-6 is distributed in the cytoplasm and nucleus, whereas QKI-7 is predominantly localized in cytoplasm (40). The QKI proteins selectively recognize a short sequence motif, ACUAAAY (where Y is pyrimidine), called the QKI response element (QRE) (41, 42). QKI proteins are also involved in the RNAi pathway. QKI interacts with Ago2 during stress responses (43). *Caenorhabditis elegans* GLD-1, a homolog of QKI, engages in both genetic and biochemical interactions with the miRNA pathway (44). In addition, QKI-7 physically interacts with GLD-2 to regulate cytoplasmic polyadenylation of specific mRNAs in a QRE-dependent manner (45). These observations prompted us to speculate that QKI-7 is involved in the selective stabilization of miR-122 mediated by GLD-2.

Here, we report that QKI-7 is involved in the stabilization of miR-122. Ago2, QKI-7, and GLD-2 form a stable ternary complex, and QKI-7 has a specific affinity for miR-122 *in vitro*. In addition, QKI-7 promoted GLD-2-mediated 3' adenylation of miR-122 *in vitro*.

Results

QKI stabilizes miR-122 in human cells

To investigate the involvement of QKI proteins in miR-122 metabolism, we knocked down QKI proteins in human Huh7 hepatoma cells using siRNA. Due to the small difference in sequence along QKI isoforms, it was impossible to knock down each isoform of QKI separately, so instead we knocked down all isoforms simultaneously. Knockdown efficiency was estimated by measuring steady-state levels of each isoform in knockdown (KD) cells, normalized against the levels in control cells (mock KD). The mRNA levels for QKI-5, QKI-6, and QKI-7 were reduced to 54, 10, and 28% of control (mock KD) levels, respectively. Although the knockdown efficiency of QKI-5 was insufficient, the levels of the cytoplasmic isoforms (QKI-6 and QKI-7) decreased markedly. The efficient knockdown of the all QKI isoforms in Huh7 cells was confirmed by immunoblotting (Fig. S1A). We observed a marked reduction of miR-122 upon QKI KD (Fig. 1A), whereas the levels of the other miRNAs (miR-21, miR-16, and miR-22) remained unchanged. In addition, we knocked down GLD-2 (to 17% of control levels), and observed down-regulation of miR-122 in GLD-2 KD cells, as reported previously (24). The decrease of miR-122 was also observed upon QKI KD with the second siRNA (si-QKI#2) (Fig. S1B). We also performed Northern blotting to analyze the steady-state levels of miRNAs and precursors in QKI or GLD-2 KD cells (Fig. 1B). A reduction of miR-122 was observed in both QKI KD cells and GLD-2 KD cells, whereas the levels of miR-122 precursor (pre-miR-122) and mature miR-21 were unchanged, indicating that depletion of QKI specifically affects the stability of miR-122 after dicing of pre-miRNA in hepatoma cells.

To investigate whether QKI stabilizes miR-122 loaded on Ago2, endogenous Ago2 was immunoprecipitated with anti-Ago2 antibody (Fig. 1C) in QKI KD Huh7 cells (Fig. S1C), and miRNAs co-precipitated with Ago2 were analyzed by real-time RT-PCR. As shown in Fig. 1D, miR-122 loaded on Ago2 was markedly decreased in QKI KD cells, when compared with the other miRNAs, showing that QKI stabilizes miR-122 loaded on Ago2.

GLD-2 interacts with QKI-7 through the nucleotidyltransferase domain

We next analyzed the subcellular localization of each QKI isoform in Huh7 cells. For this purpose, we transiently expressed QKI-FLAG proteins in Huh7 cells and performed immunostaining with anti-FLAG antibody. In Huh7 cells, QKI-5 was localized predominantly in the nucleus, whereas QKI-6 and QKI-7 were exclusively cytoplasmic (Fig. 2A); these localizations were consistent with those reported in other cell lines (30, 40).

We then conducted domain mapping of GLD-2 to determine the region of this protein required for the interaction with QKI-7. QKI-6 and QKI-7 (tagged with His₆) were recombinantly expressed in *Escherichia coli* and purified. Constructs encoding full-length GLD-2 and deletion mutants (all tagged with Myc) were transiently expressed in HEK293T cells and immunoprecipitated from cell lysate with anti-Myc antibody. The IP beads were then incubated with recombinant QKI-6 or QKI-7, followed by washing, and then the bound QKI proteins

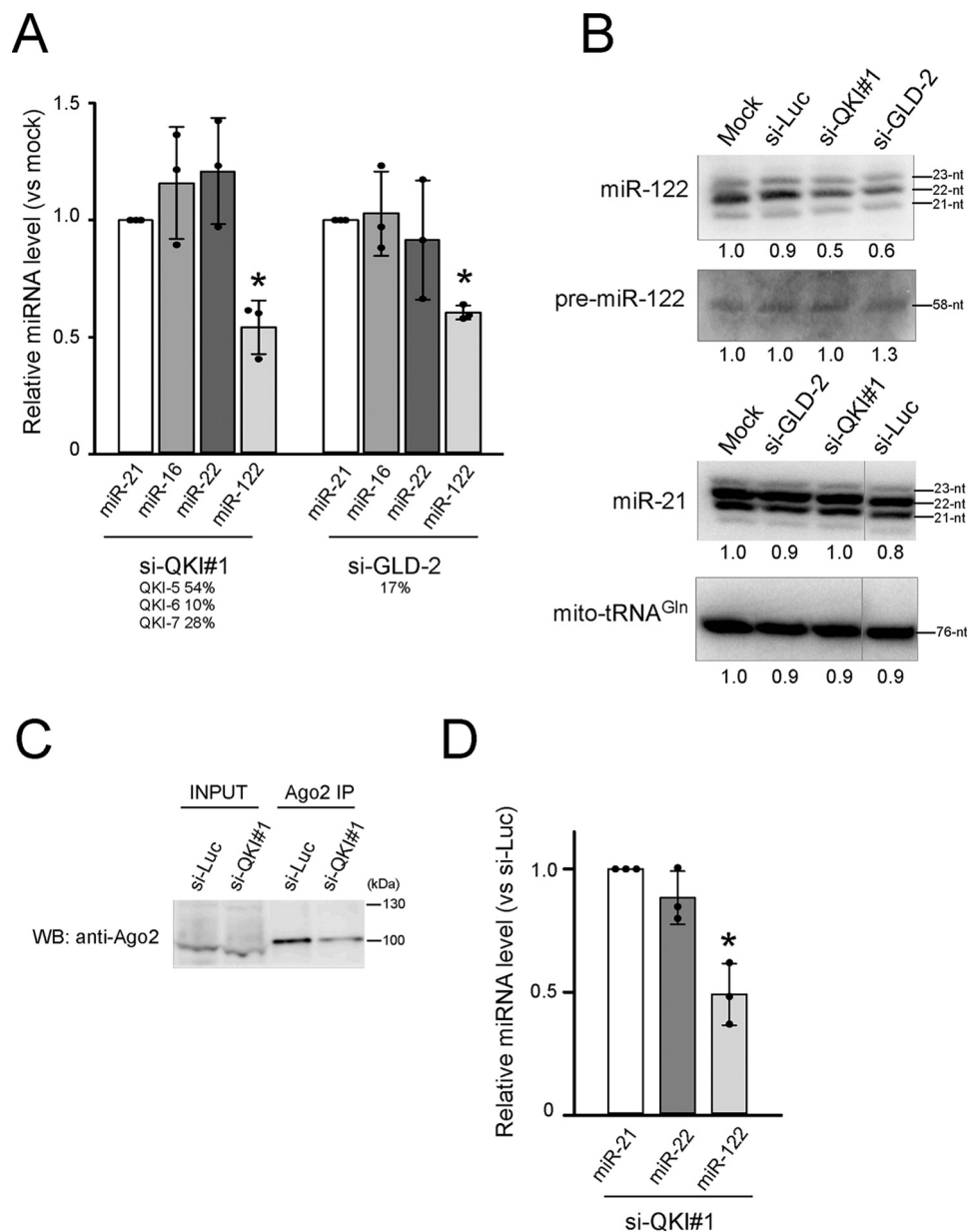


Figure 1. QKI is involved in stabilization of miR-122. *A*, steady-state levels of miRNAs upon knockdown of QKIs and GLD-2 in Huh7 cells. The values represent the ratios of the levels of each miRNA in the KD cells to those in the mock-transfected cells, as determined by real-time RT-PCR analyses, and the data were normalized against the ratio for miR-21. The error bars are S.D. Asterisks indicate statistical significance, as determined by two-tailed *t* test. *, $p < 0.05$; $n = 3$. *B*, Northern blotting of total RNA from Huh7 cells in which QKIs or GLD-2 were knocked down by siRNA (QKI KD). Knockdown of firefly luciferase (*Luc KD*) was used as a control. Band intensities are quantified and normalized against the value of mock sample. *C*, Western blot analysis of immunoprecipitated Ago2 using an anti-Ago2 antibody. *D*, real-time RT-PCR quantification of miRNAs co-immunoprecipitated with Ago2. The values represent the ratios of the levels of each Ago2-bound miRNA in the QKI KD cells (*si-QKI*) to those in control cells (*si-Luc*), and the data were normalized against the ratio for miR-21. Mean values ($n = 3$) are shown. The error bars are S.D. Asterisk indicates statistical significance, as determined by two-tailed *t* test. *, $p < 0.05$; $n = 3$.

were detected by immunoblotting. QKI-7 strongly bound to full-length GLD-2, whereas QKI-6 did not (Fig. 2*B*), suggesting that the C-terminal tail specific to QKI-7 is responsible for the interaction with GLD-2. Among the deletion constructs, only GLD-2 mutants lacking the nucleotidyltransferase (NT) domain lost the ability to interact with QKI-7, whereas the other mutants retained their ability to bind to QKI-7 (Fig. 2*B*). This result suggests that the NT domain of GLD-2 is necessary for the interaction with the C-terminal tail of QKI-7.

Finally, we examined the interaction between endogenous QKI and GLD-2 in Huh7 cells. The lysate of Huh7 was sub-

jected to immunoprecipitation with anti-GLD-2 antibody in the presence of RNases, followed by immunoblotting with anti-QKI antibody. As shown in Fig. 2*C*, endogenous QKI was specifically co-precipitated with endogenous GLD-2 independently of RNA, demonstrating that GLD-2 interacts with QKI at the physiological level in Huh7 cells.

GLD-2 interacts with Ago2 via QKI-7

QKI-6 binds to Ago2 via an interaction between the QUA2 domain (also referred to as the CK region) of QKI and the PIWI domain of Ago2 (43). Based on this knowledge, all QKI isoforms

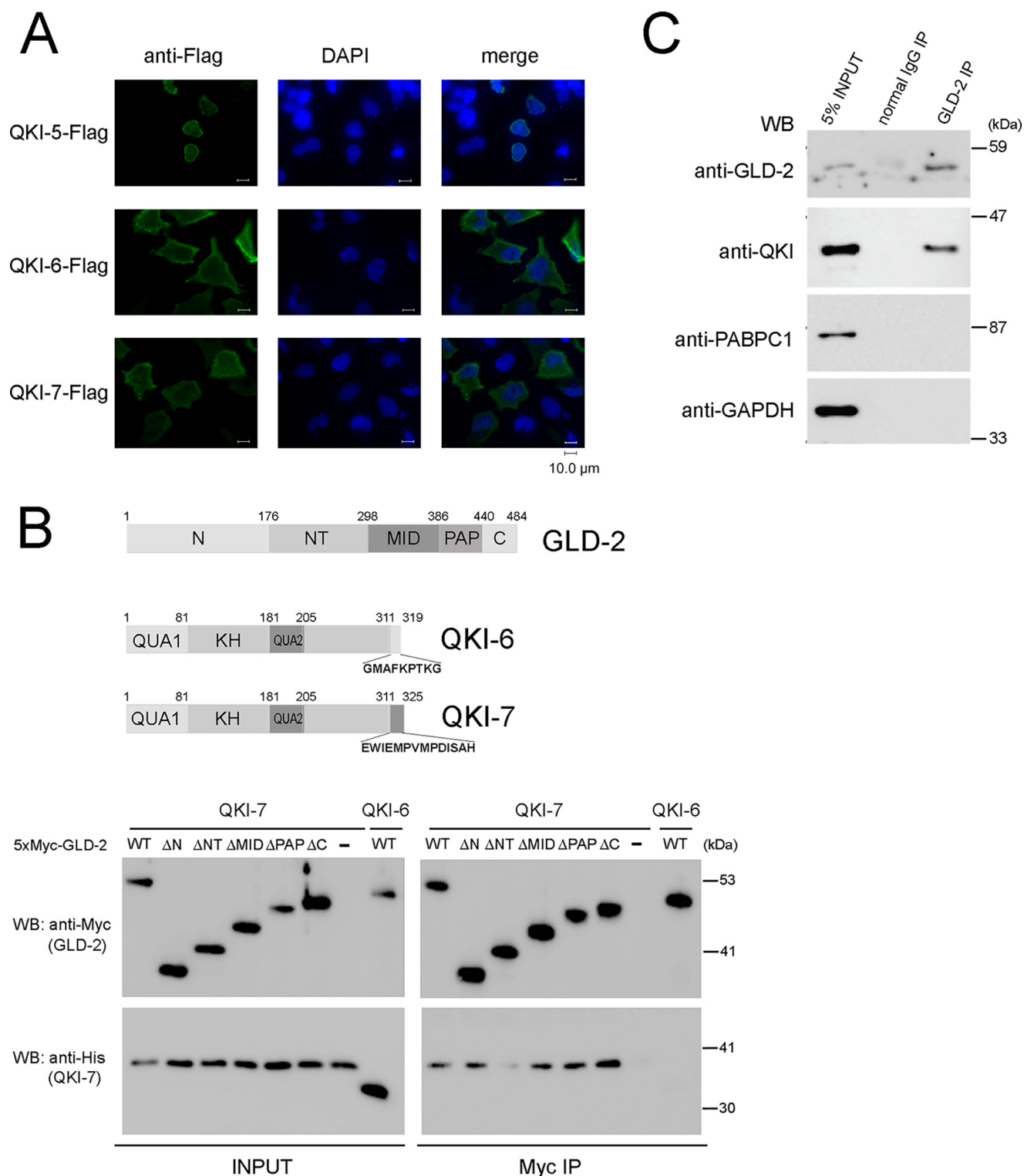


Figure 2. Subcellular localization of QKI proteins and interaction with GLD-2. *A*, subcellular localization of QKI-FLAG proteins in Huh7 cells, as determined by immunofluorescence staining using anti-FLAG antibody (green). Nuclei were stained with DAPI (blue). The green and blue images were superimposed to generate the merged panels. *B*, *in vitro* protein–protein interactions between QKI-7 and GLD-2 mutants. Myc-tagged GLD-2 variants with a truncation of each domain were immunoprecipitated in the presence of RNase A and mixed with recombinant His-QKI-7 or His-QKI-6 (INPUT). The beads were washed and analyzed by immunoblotting with the indicated antibodies (Myc IP). Domain organizations of GLD-2, QKI-6, and QKI-7 are shown in the upper panel. *C*, the interaction between endogenous GLD-2 and QKI in Huh7 cells. GLD-2 was immunoprecipitated with anti-GLD-2 antibody in the presence of RNases A and I, followed by immunoblotting with the indicated antibodies.

appear to have the ability to interact with Ago2. To test this idea, we conducted *in vitro* binding experiments using recombinant proteins. In these assays, recombinant Ago2 was cap-

tured by anti-Ago2 antibody and immobilized on protein G beads. The Ago2-bound beads were then incubated with each of the QKI isoforms, followed by washing, and then the bound

GLD-2 and QKI-7 adenylate and stabilize miRNAs

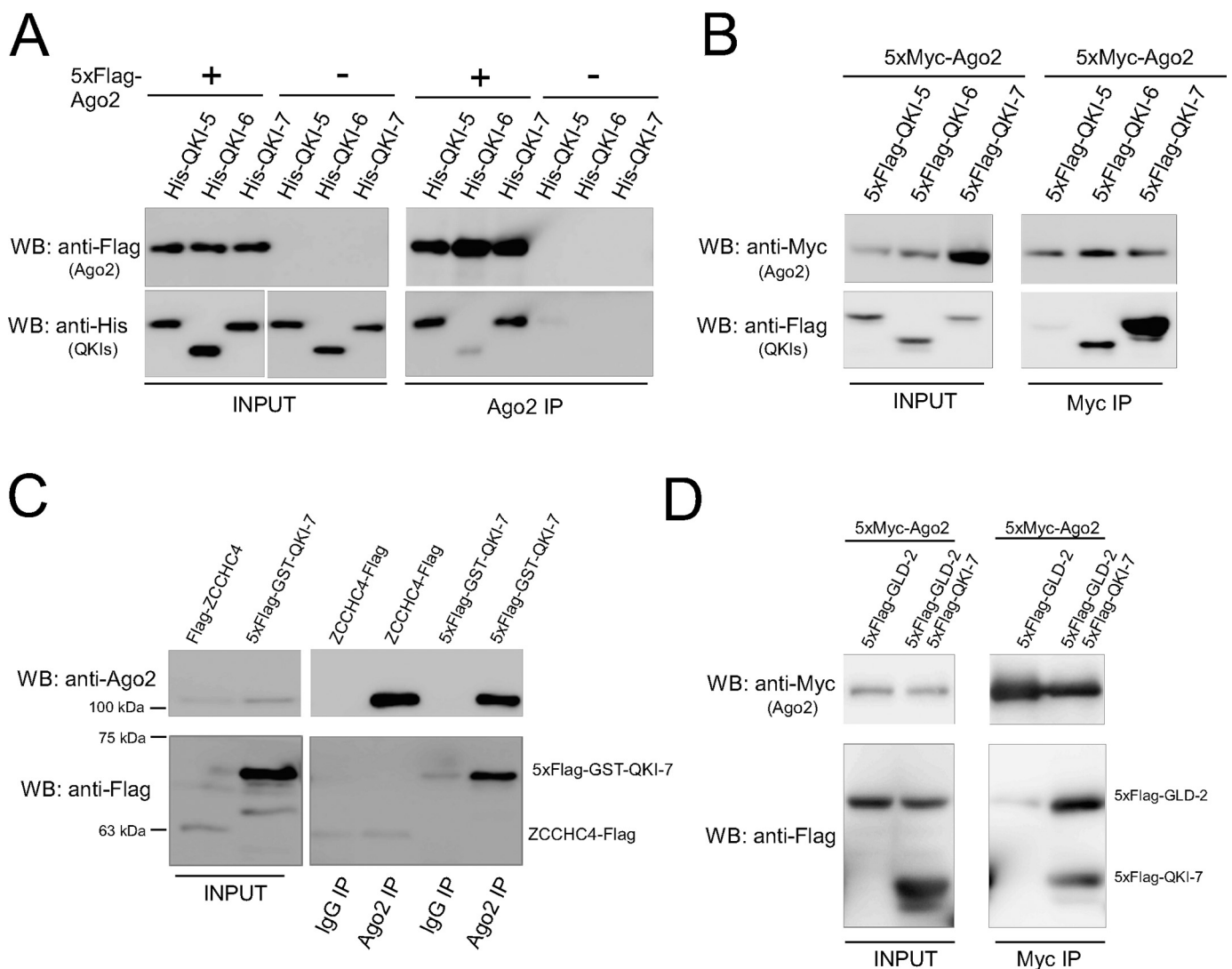


Figure 3. GLD-2 interacts with Ago2 via QKI-7. *A*, *in vitro* interaction between Ago2 and QKIs. 5×Flag-Ago2 was immobilized onto protein G beads via anti-Ago2 antibody, and then mixed with His-QKI-5, His-QKI-6, or His-QKI-7 (INPUT). The beads were washed and analyzed by immunoblotting with the indicated antibodies (Ago2 IP). As a negative control, the same experiment was performed in the absence of Ago2. Size of the relevant protein band was validated in advance. *B*, the interaction between Ago2 and QKIs in cells. HEK293T cells were co-transfected with pCMV-5×Myc-Ago2 and pCMV-5×Flag-QKI-5, pCMV-5×Flag-QKI-6, or pCMV-5×Flag-QKI-7 (INPUT). 5×Myc-Ago2 was immunoprecipitated with anti-c-Myc antibody (Myc IP), followed by immunoblotting with the indicated antibodies. Size of the relevant protein band was validated in advance. *C*, the interaction between endogenous Ago2 and overexpressed QKI-7 in Huh7 cells. Huh7 cells were transfected with pCMV-5×Flag-GST-QKI-7 or pcDNA3.1-ZCCHC4-Flag (INPUT). Endogenous Ago2 was immunoprecipitated with biotinylated anti-Ago2 antibody (Ago2 IP), followed by immunoblotting with the indicated antibodies. ZCCHC4-FLAG protein was expressed as a negative control. *D*, detection of the ternary complex consisting of Ago2, QKI-7, and GLD-2. HEK293T cells were co-transfected with pCMV-5×Myc-Ago2, pCMV-5×Flag-GLD-2, and/or pCMV-5×Flag-QKI-7 (INPUT). 5×Myc-Ago2 was immunoprecipitated with anti-c-Myc antibody in the presence of RNase A (Myc IP), followed by immunoblotting with the indicated antibodies. Size of the relevant protein band was validated in advance.

QKI protein was detected by immunoblotting. QKI-5 and QKI-7 bound strongly to Ago2 (Fig. 3A), whereas QKI-6 unexpectedly interacted much more weakly with Ago2 than the other QKI isoforms (Fig. 3A), implying that the C-terminal tail of QKI-6 plays a negative role in the interaction with Ago2. We also evaluated the interaction between Ago2 and QKI isoforms in the cell. Myc-tagged Ago2 and FLAG-tagged QKI isoforms were co-expressed in HEK293T cells, and Myc-tagged Ago2 was immunoprecipitated using anti-Myc antibody. The QKI isoforms in the co-precipitants were detected by immunoblotting. QKI-7 strongly interacted with Ago2 in the cell (Fig. 3B), whereas QKI-6 was marginally co-immunoprecipitated with Ago2, consistent with our *in vitro* binding results (Fig. 3A). QKI-5 barely co-immunoprecipitated with Ago2, likely because

this isoform is predominantly localized in the nucleus. Thus, among QKI isoforms, QKI-7 is the preferred partner for Ago2, *in vitro* as well as in the cell. Furthermore, we performed the immunoprecipitation of endogenous Ago2 in Huh7 cells in which FLAG-GST-tagged QKI-7 was expressed, and confirmed that FLAG-GST-tagged QKI-7 co-immunoprecipitates with endogenous Ago2 (Fig. 3C).

Given that QKI-7 interacted with both GLD-2 (Fig. 2, B and C) and Ago2 (Fig. 3, A–C), we hypothesized that these three proteins constitute a ternary complex, *i.e.* that GLD-2 interacts with Ago2 via QKI-7. To investigate this possibility, we analyzed the interaction between Ago2 and GLD-2 by co-immunoprecipitation in the presence or absence of QKI-7. In these experiments, Ago2 and GLD-2 were co-expressed with or with-

out QKI-7 in HEK293T cells, and Ago2 was immunoprecipitated with anti-Myc antibody. The bound GLD-2 was analyzed by immunoblotting. GLD-2 barely co-precipitated with Ago2 in the absence of QKI-7 (Fig. 3D), suggesting that GLD-2 does not physically interact with Ago2. Consistent with this finding, a previous study detected no obvious interaction between Ago2 and GLD-2 (28). On the other hand, GLD-2 was efficiently co-precipitated with Ago2 in the presence of QKI-7 (Fig. 3D), indicating that GLD-2 interacts with Ago2 via QKI-7. Because we performed the immunoprecipitation in the presence of RNase A, we could conclude that the interaction was not RNA-dependent. Thus, QKI-7, GLD-2, and Ago2 constitute an RNA-independent ternary complex.

QKI-7 interacts with miR-122 and miR-652-3p *in vitro*

To determine whether QKI-7 is involved in the selective stabilization of miR-122 mediated by GLD-2, we conducted an electrophoretic mobility shift assay (EMSA) to examine QKI-7 binding specificity toward several miRNAs, including miR-122. As shown in Fig. 4A, migration of miR-122 and miR-652-3p was clearly retarded in the presence of QKI-7 (Fig. 4A), whereas the other miRNAs tested did not interact with QKI-7. To determine the sequence element in miR-122 recognized by QKI-7, we performed EMSA with a series of miR-122 variants, each of which contained two base mutations in its sequence (Fig. 4B). Among the 11 variants, mt-1, mt-2, mt-8, and mt-10 significantly lost their ability to bind to QKI-7 (Fig. 4B), whereas the other variants exhibited interactions comparable with that of the WT sequence, indicating that the elements in miR-122 recognized by QKI-7 are dispersed among positions 1–4, 15–16, and 19–20. These elements are not related to QRE, a sequence motif recognized by QKI proteins, suggesting that QKI-7 binds to miR-122 with different mode of interaction. On the other hand, miR-652-3p has a QRE (ACUA) in the middle of the sequence, and mutation of this motif weakened affinity to QKI-7 (Fig. 4C), suggesting that miRNAs with a QRE are recognized by QKI-7.

To confirm the interaction between miR-122 and QKI-7 in the cell, QKI-7 was expressed in Huh7 cells and immunoprecipitated with anti-QKI-7 antibody (Fig. 4D). The co-precipitated RNAs were analyzed by real-time RT-PCR, showing that miR-122 was preferentially bound to QKI-7, as compared with the other miRNAs examined (Fig. 4E). This result confirmed that QKI-7 actually interacts with miR-122 in Huh7 cells.

Based on these results, we speculated that like miR-122, miR-652-3p is also stabilized by GLD-2. To test this idea, we measured the steady-state level of miR-652-3p in liver of mGLD-2^{-/-} mice by real-time quantitative RT-PCR. As described previously (24), the steady-state level of miR-122 was significantly lower in mGLD-2-null mice than in mGLD-2^{+/-} mice (Fig. 4F). The level of miR-652-3p was slightly reduced (to about 70% of control levels) in the GLD-2-null mouse (Fig. 4F), indicating that miR-652-3p, like miR-122, is also stabilized by GLD-2. Thus, the ability of QKI-7 to bind to these miRNAs contributes to the specificity of GLD-2-mediated stabilization.

QKI-7 promotes GLD-2-mediated 3' adenylation of miRNA *in vitro*

Based on these observations, we hypothesized that QKI-7 recognizes miR-122 and cooperates with GLD-2 in 3' adenylation. To test this model, we performed an *in vitro* adenylation assay with QKI-7. The presence of QKI-7 significantly facilitated the *in vitro* GLD-2-mediated adenylation of miR-122 in a dose-dependent manner (Fig. 5, A and B). By contrast, the stimulatory effect of QKI-6 (used as a negative control) was much lower than that of QKI-7 (Fig. 5, A and B). This result supports our model that QKI-7 recognizes miR-122, and recruits GLD-2 to promote selective 3' adenylation and stabilization of miR-122.

Discussion

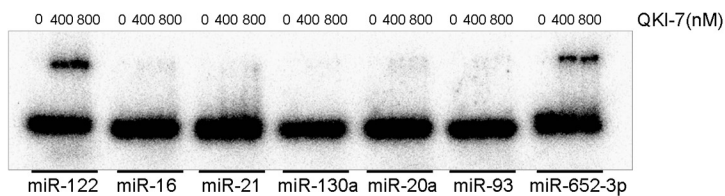
In this study, we showed that QKI-7 is involved in selective stabilization of miR-122 in hepatocytes, and that QKI-7 interacts with both GLD-2 and Ago2, forming a ternary complex. Given that GLD-2 does not have an RNA-binding domain that determines substrate specificity (46, 47), QKI-7 must act as an adaptor protein for GLD-2 to select a subset of miRNAs for 3' adenylation. Indeed, QKI-7 could recognize miR-122 and a miRNA bearing a QRE, and promoted GLD-2-mediated 3' adenylation of miR-122 *in vitro*. If the 3' adenylation takes place in the ternary complex, GLD-2 might be able to recognize the 3' terminus of Ago2-loaded miR-122 (Fig. 6). Consistent with this speculation, Wispy, a *Drosophila* homolog of GLD-2, associates with Ago1 and adenylates maternal miRNAs bound by Ago1 (48). Similarly, plant HESO1 can 3' uridylylate Ago1-bound miRNAs *in vitro* (49). According to the crystal structure of Ago2 in complex with miRNA and target RNA (50), the 3' termini of miRNAs are released from the PAZ domain of Ago protein upon binding to highly complementary target RNAs, making the 3' termini of Ago2-bound miRNAs accessible to 3' nucleotidyltransferases.

However, this model raises the question of how QKI-7 recognizes Ago2-bound miR-122 in RISC: QKI-7 interacts with the 5'-terminal region (positions 1–4) of miR-122, which should be tightly bound by the middle domain of Ago2. If the specific interaction between QKI-7 and miR-122 is essential for 3' adenylation by GLD-2, it is possible that miR-122 temporarily dissociates from Ago2 after target recognition, and subsequently is recognized by QKI-7/GLD-2 in the RISC for 3' adenylation, and is then reloaded onto Ago2 for the next round of target recognition. The RNA-binding protein AUF1 binds to let-7b and promotes its loading onto Ago2 (51). AUF1 may have the ability to capture mature miRNA and transfer it to Ago2, facilitating formation of the Ago2-miRNA complex (51). Similarly, QKI-7-GLD-2 might serve not only to prevent the release of miR-122 from RISC after target recognition, but also to facilitate reloading of miR-122 to Ago2, thereby extending the lifetime of miR-122-loaded RISC. Further investigation will be necessary to gain more detailed mechanistic insights into this process.

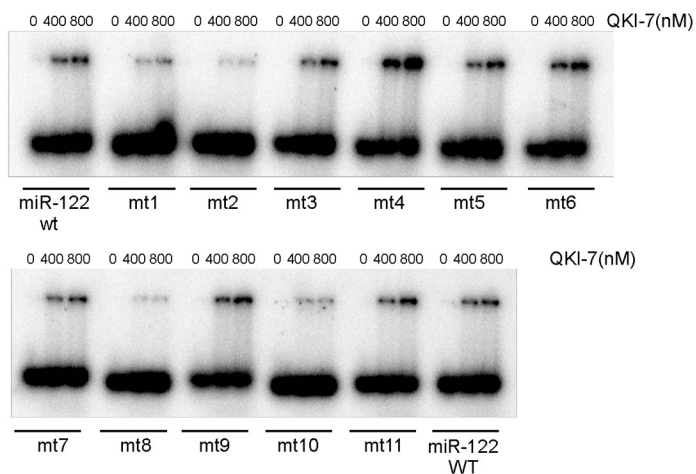
EMSA analysis revealed that QKI-7 recognizes miR-652-3p as well as miR-122. miR-652-3p has a partial QRE motif, and a miR-652-3p variant with a mutation in the QRE was not

GLD-2 and QKI-7 adenylate and stabilize miRNAs

A

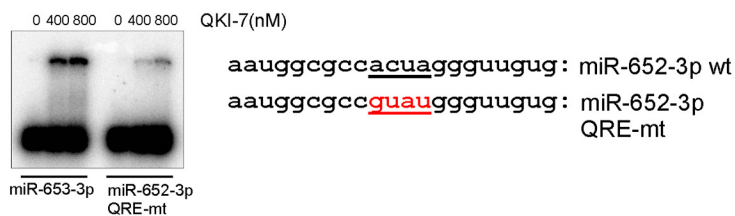


B

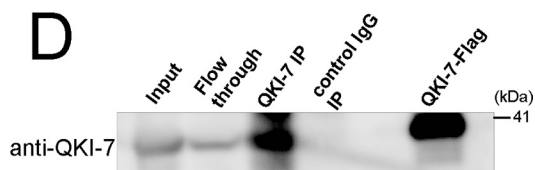


uggagugugacaauggguguuug: miR-122 wt
 cagagugugacaauggguguuug: mt-1
 ugaggugugacaauggguguuug: mt-2
 uggaaggugacaauggguguuug: mt-3
 uggaguaacgacaauggguguuug: mt-4
 uggaguguagcaaauggguguuug: mt-5
 uggagugugaguauuggguguuug: mt-6
 uggagugugacagcggguguuug: mt-7
 uggagugugacaaucuuuguuug: mt-8
 uggagugugacaaugggauuug: mt-9
 uggagugugacaaugggugccug: mt-10
 uggagugugacaauggguguuga: mt-11

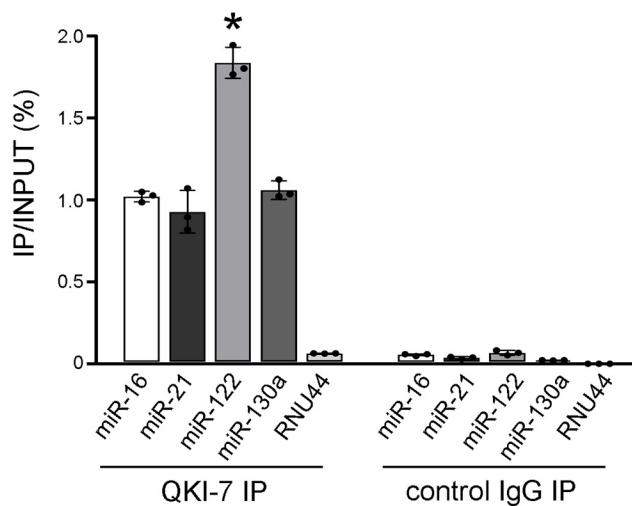
C



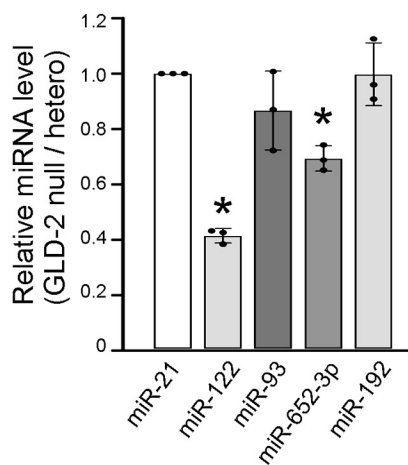
D



E



F



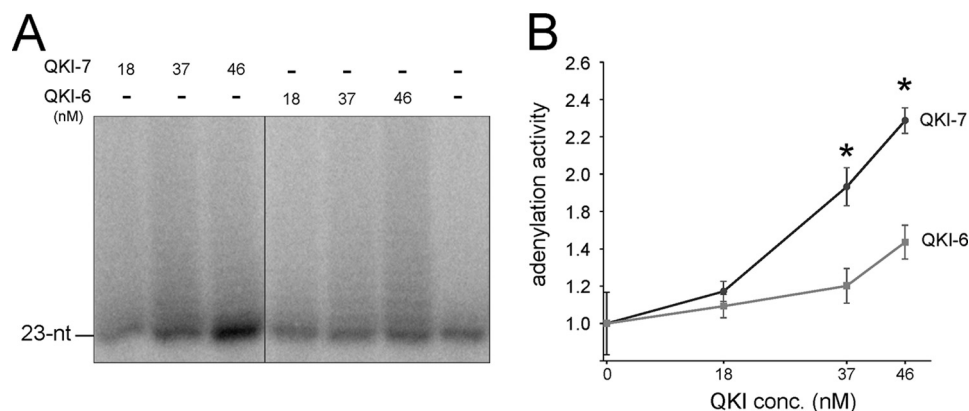


Figure 5. QKI-7 promotes GLD-2-mediated 3' adenylation of miR-122 *in vitro*. *A*, *in vitro* adenylation of miR-122 (22 nucleotides) by recombinant GLD-2 (1.3 nM) in the absence or presence of recombinant HA-QKI-7 (18–46 nM) or HA-QKI-6 (18–46 nM). An aliquot of the reaction mixture was analyzed by 13% denaturing PAGE. *B*, quantification of the results shown in *A*. Data are presented as mean \pm S.D., and asterisks indicate statistical significance as determined by two-tailed *t* test. *, $p < 0.005$; $n = 3$.

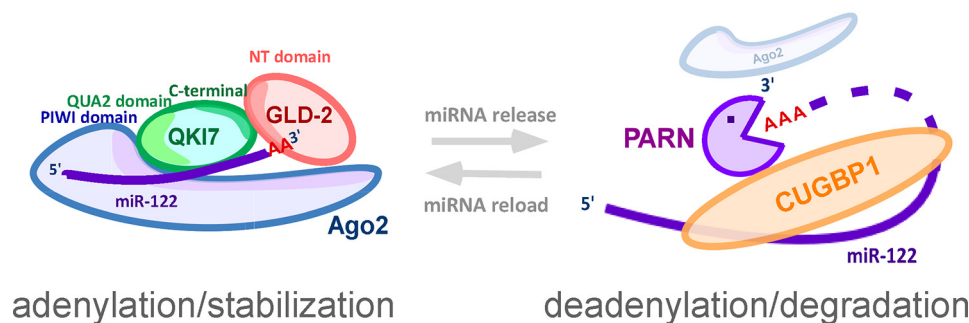


Figure 6. Mechanistic insights into miRNA metabolism mediated by 3'-oligoadenylation and deadenylation. The schematic depiction of miR-122 metabolism regulated by 3' adenylation. In the RISC containing QKI-7 and GLD-2, GLD-2 in concert with QKI-7 specifically adenylates and stabilizes miR-122 in proximity to Ago2. In this complex, QKI-7 interacts with GLD-2 via the C-terminal region of QKI-7 and NT domain of GLD-2, and the QUA2 domain of QKI-7 contacts with the PIWI domain of Ago2. Following dissociation of miR-122 from the RISC, the miRNA is trapped by the CUGBP1/PARN complex for deadenylation and degradation. A subpopulation of the shortened miRNAs might be transferred to QKI-7/GLD-2 and reloaded onto Ago2. Thus, the opposing effects of QKI-7/GLD-2 and PARN/CUGBP1 determine the steady-state level of miR-122.

efficiently recognized by QKI-7, suggesting that QKI-7 recognizes this miRNA in a similar fashion to QRE-containing mRNAs, and that other miRNAs containing QREs could be recognized and regulated by QKI-7. By contrast, miR-122 has no QRE, and EMSA revealed that QKI-7 recognizes dispersed regions of miR-122 that do not correspond to the motifs recognized by QKI (41, 42). This finding indicates that sequence elements recognized by QKI proteins have greater diversity than previously thought. Notably in this regard, QKI proteins are involved in stabilization of mature miR-20a, which does not have a QRE (52). Because miR-20a targets TGFBR2, an oncogene involved in gliomagenesis, QKI acts as a tumor suppressor by stabilizing miR-20a (52). Although the precise mechanism of QKI-mediated stabilization of miR-20a has not been elucidated, the possible

involvement of GLD-2 should be investigated. Intriguingly, GLD-1, a homolog of QKI in *C. elegans*, interacts genetically with the miR-35 and let-7 pathways. In addition, *C. elegans* GLD-1 physically interacts with proteins required for miRNA pathways (44). Thus, our findings in this study provide insights into the function of GLD-1 in the miRNA pathways of *C. elegans*.

Multiple instances of 3' adenylation of miRNA have been reported. In mammalian and fly cells infected by poxvirus, viral poly(A) polymerase VP55 mediates 3' adenylation of host miRNAs (53). Mammalian PAPD5 adenylates the 3' end of miR-21 (54), whereas in fly, the noncanonical poly(A) polymerase Wispy is responsible for 3' adenylation of maternally inherited miRNAs (48). In all of these cases, miRNAs are destabilized by 3' adenylation, whereas miR-122 is stabilized by GLD-2–

Figure 4. QKI-7 specifically binds to miR-122 and miR-652-3p *in vitro*. *A*, EMSAs to detect the interaction between QKI-7 and miRNAs. Each 5'-³²P-labeled miRNA (20 nM) was mixed with QKI-7-FLAG protein (0, 400, or 800 nM), and the complex was detected by EMSA. *B*, EMSAs to determine residues of miR-122 involved in the QKI-7 interaction. Sequences of miR-122 mutants are shown on the right panel; the mutated residues in each mutant are shown in red. Each 5'-³²P-labeled miRNA (20 nM) was mixed with QKI-7-FLAG protein (0, 400, or 800 nM), and the complex was detected by EMSA. Blue letters on miR-122 (right panel) indicate critical residues for QKI-7 recognition, as determined in this experiment. *C*, EMSAs to examine QRE mutations in miR-652-3p. Sequences of miR-652-3p and its QRE mutant are shown on the right. QRE and its mutation (red) are underlined. Each 5'-³²P-labeled miRNA (20 nM) was mixed with QKI-7-FLAG protein (0, 400, or 800 nM), and the complex was detected by EMSA. *D*, Western blot analysis of immunoprecipitated QKI-7 using an anti-QKI-7 antibody. *E*, real-time RT-PCR quantification of miRNAs and small nucleolar RNA RNU44 co-immunoprecipitated with QKI-7 or IgG as a control. Mean values ($n = 3$) are shown. The error bars are S.D. Asterisk indicates statistical significance, as determined by two-tailed *t* test. *, $p < 0.005$; $n = 3$. *F*, ratio of the steady-state level of each miRNA in the liver of mGLD-2^{-/-} mice versus mGLD-2^{+/-} mice, measured by real-time RT-PCR. Each ratio was normalized against that of miR-21. Mean values ($n = 3$) are shown. The error bars are S.D. Asterisks indicate statistical significance as determined by two-tailed *t* test. *, $p < 0.05$; $n = 3$.

GLD-2 and QKI-7 adenylate and stabilize miRNAs

mediated 3' adenylation. Therefore, unlike 3' uridylation of miRNAs, 3' adenylation of miRNAs does not have a consistent functional meaning.

Recent work showed that QKI-7, in cooperation with GLD-2, regulates cytoplasmic polyadenylation and translation of the specific mRNAs in a QRE-dependent manner (45). Taken together with our finding in this study that QKI-7/GLD-2 also mediates 3' adenylation of a subset of miRNAs, we propose that QKI-7/GLD-2 controls translation of specific mRNAs via two distinct pathways: regulatory translation of mRNAs by cytoplasmic polyadenylation and stabilization of miRNAs by 3' adenylation. These findings should help to elucidate the molecular pathogenesis of human diseases caused by dysregulation of QKI proteins.

Based on the results of this study along with our previous observations, we propose a current model for the regulation of miRNA metabolism mediated by adenylation and deadenylation (Fig. 6). In the RISC containing QKI-7 and GLD-2, miR-122 and other miRNAs (including miR-652-3p) are 3'-oligoadenylated and specifically stabilized. After target recognition, oligoadenylated miRNAs are dissociated from the RISC and trapped by the CUGBP1/PARN complex for deadenylation. Some populations of shortened miRNAs are transferred to QKI-7/GLD-2 and reloaded onto Ago2, whereas others are subjected to degradation. Thus, the opposing effects of QKI-7/GLD-2 and PARN/CUGBP1 balance the cellular levels of miR-122 and other miRNAs.

Experimental procedures

RNAi and real-time RT-PCR

Huh7 cells were cultured in 10-cm dishes in Dulbecco's modified Eagle's medium/F-12 containing 10% fetal bovine serum and transfected with siRNAs (1 nM) using Lipofectamine RNAiMAX (Invitrogen). Target sequences of the siRNAs were designed using the siExplorer algorithm (55). The sense strand sequences of the siRNAs for GLD-2, QKI, and firefly luciferase (control) are provided in Table S1. Mock transfection was performed by the same procedure in the absence of siRNA. Seventy-two hours after transfection, the cells were treated with Tri-Pure (Roche) to isolate total RNA. The efficiency of gene silencing was confirmed by real-time RT-PCR. Specifically, total RNA was treated with 2 units of RQ1 DNase (Promega) at 37 °C for 30 min in a 20- μ l reaction mixture, and then RQ1 DNase stop solution was added. Reverse transcription was performed in a solution containing DNase-treated RNA, oligo(dT) primer, random N6 primer, and 20 units of Transcriptor reverse transcriptase (Roche). The reaction was incubated at 55 °C for 30 min, and then the reverse transcriptase was inactivated by heating at 85 °C for 5 min. One microliter of the cDNA solution was used as a template for real-time PCRs on a Light-Cycler 480 Real-time PCR System (Roche). The thermal cycling conditions were as follows: 45 cycles of 95 °C for 10 s, 58 °C for 12 s, and 72 °C for 7 s. The sequences of the quantitative PCR primers are provided in Table S1. The expression levels of mature miRNAs were measured using TaqMan miRNA assays (Applied Biosystems).

Northern blotting

Total RNA was separated by 20% denaturing PAGE and transferred to Hybond-N⁺ membrane (GE Healthcare) using a semidry Trans-Blot SD (Bio-Rad). Locked nucleic acid probes were phosphorylated with [γ -³²P]ATP (PerkinElmer Life Sciences) using T4 polynucleotide kinase (Toyobo). The membrane was UV cross-linked and hybridized with 5'-³²P-radiolabeled locked nucleic acid probes overnight at 50 °C in PerfectHyb solution (Toyobo). The sequences of the probes are listed in Table S1. The membranes were exposed to an imaging plate (Fujifilm), and radioactivity was visualized using an FLA7000 Image Analyzer (Fujifilm). Full-size images for blot data are presented in Fig. S2.

Plasmid construction

The procedures for construction of pCMV-5 \times Flag-QKI-5, -6, -7, GLD-2, and pCMV-5 \times Myc-GLD-2 were described previously (45). To construct pCMV-5 \times Flag(Myc)-Ago2, the ORF of Ago2 was PCR-amplified and inserted into the EcoRI and Sall sites of pCMV-5 \times Flag(Myc). To construct pCMV-5 \times Flag-Tev-GLD-2, the tobacco etch virus site sequence was inserted into pCMV-5 \times Flag-GLD-2 by QuikChange mutagenesis (Agilent). The series of pCMV-5 \times Myc-GLD-2 mutants were constructed based on pCMV-5 \times Myc-GLD-2 via the QuikChange reaction. To construct pCMV-HA-QKI-6 or pCMV-HA-QKI-7, vector pCMV-HA was generated by the QuikChange reaction using pCMV-5 \times Myc-GLD-2 as a template. Then, the ORF of QKI-6 or QKI-7 was PCR-amplified and inserted into the EcoRI and Sall sites of pCMV-HA. To construct pDEST12.2-QKI-5, -6, and -7, the corresponding ORFs were PCR-amplified and cloned into vector pENTR. Subsequently, pDEST12.2-Flag and the corresponding pENTR vectors. To construct pET28a-QKI-5, -6, and -7, the corresponding ORFs were PCR-amplified and inserted into the NheI and HindIII sites of pET-28a. To construct pCMV-5 \times Flag-GST-QKI-7, GST sequence was inserted to pCMV-5 \times Flag-QKI-7 by SLICE reaction (56). The sequences of the primers used in vector constructions are provided in Table S1.

Vector transfection

For transfection of pDEST12.2-QKI-Flag vectors (Fig. 2A), Huh7 cells cultured in 35-mm dishes were transfected with 1 μ g of vector using FuGENE (Roche) (4.2 μ l). For transfection of pCMV-5 \times Flag-GST-QKI-7 vector (Fig. 3C), Huh7 cells (1.5×10^7 cells) were transfected with 6 μ g of vector using Lipofectamine 2000 (Invitrogen). For other transfection experiments, HEK293T cells were used. For transfection of pDEST12.2-QKI-7-Flag or pCMV-5 \times Flag-Ago2, HEK293T cells (1×10^7 cells) were transfected with 40 μ g of vector using polyethylenimine (90 μ l) and cultured for 48 h. For transfection of pCMV-HA-QKI-6 or pCMV-HA-QKI-7, HEK293T cells (1×10^7 cells) were transfected with 12 μ g of vector using polyethylenimine (96 μ l) and cultured for 48 h. For transfection of pCMV-5 \times FLAG-Tev-GLD-2, pCMV-5 \times Myc-GLD-2, pCMV-5 \times Myc-Ago2, pCMV-5 \times Flag-QKI-5, pCMV-5 \times Flag-QKI-6, and pCMV-5 \times Flag-QKI-7, HEK293T cells (1×10^7

cells) were transfected with 12 μg of vector using Lipofectamine 2000 (Invitrogen) (12 μl) and cultured for 48 h.

Immunoprecipitation

Except for the experiments shown in Figs. 2C and 3C, cells were suspended in lysis buffer A (150 mM KCl, 10 mM Tris-HCl (pH 8.0), 2.5 mM MgCl_2 , 1 mM DTT, 0.5% Triton X-100, and Complete Mini Protease Inhibitor Mixture Tablet (Roche)), and lysed by passing through a 25-gauge needle on a syringe a total of 10 times. The lysate was centrifuged twice at $20,000 \times g$ for 20 min to remove cell debris. The supernatant was mixed with anti-FLAG M2-agarose beads (Sigma-Aldrich), anti-c-Myc antibody beads (Wako), or anti-HA-agarose beads (Wako), anti-Ago2 antibody (Wako) and rotated at 4 °C for 2–5 h. The beads were washed three times with wash buffer (300 mM KCl, 10 mM Tris-HCl (pH 8.0), 2.5 mM MgCl_2 , 0.5% Triton X-100, and 1 mM DTT). QKI-7-Flag or 5 \times Flag-Ago2 was eluted from the beads with FLAG peptide in elution buffer (150 mM KCl, 10 mM Tris-HCl (pH 8.0), 20% glycerol, 1 mM DTT, and 200 $\mu\text{g}/\text{ml}$ of 3 \times FLAG peptide (Sigma)), and then concentrated using an Amicon Ultra YM-10 filter (Millipore). HA-QKI-6 or HA-QKI-7 were eluted from the beads with HA peptide in elution buffer (10 mM Tris-HCl (pH 8.0), 150 mM KCl, 20% glycerol, 1 mM DTT, and 500 $\mu\text{g}/\text{ml}$ of HA peptide (Wako)), and then dialyzed overnight against dialysis buffer (10 mM Tris-HCl (pH 8.0), 150 mM KCl, 20% glycerol, and 1 mM DTT) to remove HA peptide. GLD-2 used in the *in vitro* adenylation assay was eluted from FLAG-agarose beads using ProTEV Plus protease (0.13 units/ μl) (Promega).

For the co-immunoprecipitation assay shown in Fig. 2C, Huh7 cells grown in four 10-cm dishes were washed twice with PBS and lysed in 1 ml of lysis buffer (20 mM Tris-HCl at pH 7.5, 100 mM NaCl, 2.5 mM EDTA, 0.5% Nonidet P-40, 1 \times protease inhibitor mixture (Nacalai), 5 $\mu\text{g}/\text{ml}$ of RNase A, 50 units/ml of RNase If (New England Biolabs)), followed by incubation at 37 °C for 10 min and then on ice for 10 min. The lysates were centrifuged at 15,000 rpm ($20,400 \times g$) for 20 min at 4 °C, and supernatants were collected in a new tube. 500- μl aliquots were mixed with 2 μg of GLD-2 antibody (N-15; sc-168897 Santa Cruz) or normal goat IgG (sc-2028 Santa Cruz) and rotated for 3 h with protein G-Sepharose (GE healthcare) pre-equilibrated with lysis buffer. The beads were then washed three times with lysis buffer, and proteins retained on the resin were subjected to Western blot analysis.

For Ago2 immunoprecipitation as shown in Fig. 3C, Huh7 cells were suspended in lysis buffer A and lysed by passing through a 25-gauge needle. The lysate was centrifuged twice at $20,000 \times g$ for 20 min to remove cell debris. Anti-Ago2 antibody (Wako, 281-81251) biotinylated using EZLink NHS Biotin (Thermo number 20217) was incubated with Dynabeads Myone Streptavidin C1 (DynaL DB65001). The antibody-bound beads were mixed with Huh7 lysate and rotated at 4 °C overnight. The beads were washed with lysis buffer A and proteins retained on the beads were subjected to Western blot analysis. Normal mouse IgG (Santa Cruz, sc-2025) was used as control.

RNP IP and real-time RT-PCR

To analyze Ago2-loaded miRNAs (Fig. 1, C and D), Huh7 cells were transfected with siRNAs (1 nM) using RNAiMAX (Invitrogen). Seventy-two hours after transfection, cells were suspended in lysis buffer A, and Ago2 was immunoprecipitated using anti-Ago2 antibody (Wako, 281–81251) and protein G Dynabeads (DynaL, DB10003). The beads were washed with lysis buffer A, and the beads were treated with TRIzol (ThermoFisher) to isolate the bound RNAs. The obtained RNAs were analyzed by real-time RT-PCR.

To analyze QKI-7 bound miRNAs (Fig. 4, D and E), Huh7 cells transfected with pDEST12.2-QKI-7-Flag were suspended in lysis buffer A including SUPERnase-IN (Ambion). The lysate was mixed with protein G 4 Fast Flow (GE Healthcare) (100 μl) and rotated for 1 h, and the supernatants were collected as precleared lysate. Anti-QKI-7 antibody (Millipore, AB9908) or normal rabbit IgG (5 μg) was mixed with precleared lysate in the presence of protein G 4 Fast Flow (60 μl), and immunoprecipitation was performed for 3 h. The beads were washed with lysis buffer A, and the immunoprecipitates or INPUT lysate were treated with Tripure (Roche) to isolate the bound RNAs. The obtained RNAs were analyzed by real-time RT-PCR.

Purification of the recombinant proteins

To generate recombinant His-QKI proteins, the *E. coli* Rosetta strain was transformed with each plasmid (pET28a-QKI-5, pET28a-QKI-6, and pET28a-QKI-7) and cultured in Luria-Bertani medium containing 50 $\mu\text{g}/\text{ml}$ of kanamycin and 50 $\mu\text{g}/\text{ml}$ of chloramphenicol. When the OD_{600} of the transformants reached 0.6, protein expression was induced by the addition of 0.1 mM isopropyl 1-thio- β -D-galactopyranoside, and the cells were cultured for an additional 4 h at 37 °C. The cells were harvested and suspended in buffer L (20 mM HEPES-KOH (pH 7.6), 300 mM KCl, 1 mM phenylmethylsulfonyl fluoride, and 2 mM β -mercaptoethanol), and then disrupted by sonication on ice. The cell lysate was cleared by ultracentrifugation at 45,000 rpm ($100,000 \times g$) for 60 min. Recombinant His-QKI proteins were purified using the AKTA Chromatography System and a His-trap column (GE Healthcare). Fractions containing the recombinant proteins were pooled and dialyzed overnight against buffer A (20 mM HEPES-KOH (pH 7.6), 50 mM KCl, and 1.4 mM β -mercaptoethanol). The QKI proteins were further purified by an anion exchange chromatography using a Mono Q column (GE Healthcare). Fractions containing the recombinant proteins were pooled and dialyzed overnight against buffer B (20 mM HEPES-KOH (pH 7.6), 100 mM KCl, 1.4 mM β -mercaptoethanol, and 10% glycerol).

In vitro protein interaction

To analyze the interaction between GLD-2 mutants and QKI-7 (Fig. 2B), a series of Myc-tagged GLD-2 variants harboring truncations of each domain were immunoprecipitated with anti-c-Myc antibody beads (Wako) in the presence of RNase A (1 $\mu\text{g}/\text{ml}$). Approximately 2.4 pmol of GLD-2 mutants immobilized on anti-c-Myc antibody beads were mixed with 24 pmol His-QKI-7 or His-QKI-6 in binding buffer (150 mM KCl, 10 mM Tris-HCl (pH 8.0), 2.5 mM MgCl_2 , 0.2 mM DTT, and 0.1% Triton X-100) and incubated at 30 °C for 1 h. The beads were

GLD-2 and QKI-7 adenylate and stabilize miRNAs

washed three times with wash buffer (250 mM KCl, 10 mM Tris-HCl (pH 8.0), 2.5 mM MgCl₂, 0.2 mM DTT, and 0.1% Triton X-100) and analyzed by immunoblotting.

To analyze the interaction between Ago2 and QKI (Fig. 3A), 5× FLAG-Ago2 (16 pmol) was immunoprecipitated using anti-Ago2 antibody (4G8; Wako) (20 μl) and protein G-Sepharose (50 μl) in 200 μl of IP buffer (100 mM KCl, 10 mM Tris-HCl (pH 8.0), 2.5 mM MgCl₂, 1 mM DTT, and 0.1% Triton X-100). After incubation at 4 °C for 2 h, the beads were washed three times with IP buffer, and the volume was adjusted to a 50% slurry. 5× FLAG-Ago2 beads (12 μl) were mixed with His-QKI-5, His-QKI-6, or His-QKI-7 (10 pmol) in 100 μl of IP buffer, and then incubated at 30 °C for 1 h. Finally, the beads were washed three times with IP buffer and analyzed by immunoblotting.

Antibodies

Immunoblotting was performed using anti-Pan-QKI clone N147/6 (1:750, MABN624, Merck) (Fig. S1, A and C), anti-DDDDK tag mAb-HRP-Direct (1:5000, M185-7, MBL) (Fig. 3, A–D), anti-DYKDDDDK tag antibody (Wako 018-22381) (Fig. 3C), anti-Myc tag mAb-HRP-Direct (1:2000, M192-7, MBL), anti-His tag mAb-HRP-Direct (1:2000, D291-7, MBL), and anti-QKI-7 antibody (1:500, AB9908, Millipore) (Fig. 4D). The details of anti-QKI (Fig. 2C) and anti-GAPDH antibodies (Fig. 2C) are described previously (45). Anti-GLD-2 (Fig. 2C) and anti-PABPC1 (Fig. 2C) antibodies were raised against His-tagged GLD-2 and His-tagged PABPC1, respectively. These antibodies were validated for Western blotting using lysates obtained from siPAPD4- or siPABPC1-treated cells. Full-size images for blot data are presented in Fig. S2.

Immunostaining

Huh7 cells were transfected with a series of pDEST12.2-QKI using FuGENE (Roche). Twenty-four hours after transfection, the cells were washed with PBS and then fixed with 3.7% formaldehyde in PBS for 30 min at room temperature. The fixed cells were washed three times with PBS, permeabilized with 0.5% Triton in PBS for 10 min at room temperature, and blocked with 2% fetal bovine serum in PBS for 30 min at room temperature. The blocked cells were incubated for 1 h at room temperature with mouse anti-FLAG antibody (1:500; Sigma, F1804) diluted in Can Get Signal solution A (Toyobo), and then for an additional 1 h at room temperature with Alexa Fluor 488-conjugated anti-mouse secondary antibody (1:1000; Invitrogen, A-11029) diluted in Can Get Signal solution A. Nuclei were stained with DAPI. Fluorescence images were acquired on a Leica DMI6000B microscope equipped with a DFC360FX cooled CCD camera. Images were processed using the AF6500 software (Leica).

Electrophoretic mobility shift assays

5'-³²P-labeled miRNAs (20 nM) were mixed with the indicated concentrations of QKI-7-FLAG (0–800 nM) in a mixture containing 20 mM HEPES-KOH (pH 7.6), 100 mM KCl, 2 mM MgCl₂, 8% glycerol, and RNasin RNase inhibitor (Promega). The mixture was incubated at 30 °C for 30 min. After addition of a 25% volume of loading dye (50 mM Tris-HCl (pH 8.0) and

5 mM Mg(OAc)₂), each sample was analyzed by 5% native PAGE at 4 °C and visualized on an FLA7000 Image Analyzer (Fujifilm).

In vitro adenylation

Prior to the reaction, GLD-2 (6.5 nM) was incubated with HA-QKI-7 (0–230 nM) or HA-QKI-6 (0–230 nM) at 30 °C for 20 min in a buffer containing 20 mM HEPES-KOH (pH 7.6), 100 mM KCl, and 1 mM DTT. Next, 3 μl of the mixture was added to 12 μl of a solution containing synthetic miR-122 (10 nM), 20 mM Tris-HCl (pH 8.0), 50 mM KCl, 2 mM MgCl₂, 2 mM MnCl₂, 50 μg/ml of BSA, and 43 nM (4.8 kBq/μl) [α -³²P]ATP (PerkinElmer). The reaction was incubated at 37 °C for 15 min. The miRNA was extracted from the mixture by phenol/chloroform treatment, and then analyzed by 13% denaturing PAGE. The radioactivity of the labeled miRNAs was visualized on an FLA7000 Image Analyzer (Fujifilm).

Author contributions—H. H., Y. Y., and T. S. conceptualization; H. H., Y. Y., Y. N., K. O., R. Y., S. O., and S.-i. H. data curation; H. H., Y. Y., Y. N., K. O., R. Y., S. O., and S.-i. H. formal analysis; H. H. and T. S. supervision; H. H., Y. Y., Y. N., K. O., R. Y., S. O., and T. S. investigation; H. H. and Y. Y. writing-original draft; H. H. and T. S. project administration; K. O., R. Y., S. O., and S.-i. H. resources.

Acknowledgments—We are grateful to the members of the Suzuki laboratory for providing materials, technical assistance, and fruitful discussions. Special thanks are due to Dr. Takayuki Katoh (University of Tokyo) for technical support and advice and Drs. Tadashi Baba and Shin-ichi Kashiwabara (Tsukuba University) for providing materials.

References

1. Bartel, D. P. (2009) MicroRNAs: target recognition and regulatory functions. *Cell* **136**, 215–233 [CrossRef Medline](#)
2. Guo, H., Ingolia, N. T., Weissman, J. S., and Bartel, D. P. (2010) Mammalian microRNAs predominantly act to decrease target mRNA levels. *Nature* **466**, 835–840 [CrossRef Medline](#)
3. Ha, M., and Kim, V. N. (2014) Regulation of microRNA biogenesis. *Nat. Rev. Mol. Cell Biol.* **15**, 509–524 [CrossRef Medline](#)
4. Ameres, S. L., and Zamore, P. D. (2013) Diversifying microRNA sequence and function. *Nat. Rev. Mol. Cell Biol.* **14**, 475–488 [CrossRef Medline](#)
5. Krol, J., Loedige, I., and Filipowicz, W. (2010) The widespread regulation of microRNA biogenesis, function and decay. *Nat. Rev. Genet.* **11**, 597–610 [CrossRef Medline](#)
6. Heo, I., Joo, C., Cho, J., Ha, M., Han, J., and Kim, V. N. (2008) Lin28 mediates the terminal uridylation of let-7 precursor MicroRNA. *Mol. Cell* **32**, 276–284 [CrossRef Medline](#)
7. Heo, I., Joo, C., Kim, Y. K., Ha, M., Yoon, M. J., Cho, J., Yeom, K. H., Han, J., and Kim, V. N. (2009) TUT4 in concert with Lin28 suppresses microRNA biogenesis through pre-microRNA uridylation. *Cell* **138**, 696–708 [CrossRef Medline](#)
8. Thornton, J. E., Chang, H. M., Piskounova, E., and Gregory, R. I. (2012) Lin28-mediated control of let-7 microRNA expression by alternative TUTases Zcchc11 (TUT4) and Zcchc6 (TUT7). *RNA* **18**, 1875–1885 [CrossRef Medline](#)
9. Chang, H. M., Triboulet, R., Thornton, J. E., and Gregory, R. I. (2013) A role for the Perlman syndrome exonuclease Dis3l2 in the Lin28-let-7 pathway. *Nature* **497**, 244–248 [CrossRef Medline](#)
10. Heo, I., Ha, M., Lim, J., Yoon, M. J., Park, J. E., Kwon, S. C., Chang, H., and Kim, V. N. (2012) Mono-uridylation of pre-microRNA as a key step in the biogenesis of group II let-7 microRNAs. *Cell* **151**, 521–532 [CrossRef Medline](#)

11. Yu, B., Yang, Z., Li, J., Minakhina, S., Yang, M., Padgett, R. W., Steward, R., and Chen, X. (2005) Methylation as a crucial step in plant microRNA biogenesis. *Science* **307**, 932–935 [CrossRef Medline](#)
12. Ren, G., Chen, X., and Yu, B. (2012) Uridylation of miRNAs by hen1 suppressor1 in *Arabidopsis*. *Curr. Biol.* **22**, 695–700 [CrossRef Medline](#)
13. Zhao, Y., Yu, Y., Zhai, J., Ramachandran, V., Dinh, T. T., Meyers, B. C., Mo, B., and Chen, X. (2012) The *Arabidopsis* nucleotidyl transferase HESO1 uridylylates unmethylated small RNAs to trigger their degradation. *Curr. Biol.* **22**, 689–694 [CrossRef Medline](#)
14. Ramachandran, V., and Chen, X. (2008) Degradation of microRNAs by a family of exoribonucleases in *Arabidopsis*. *Science* **321**, 1490–1492 [CrossRef Medline](#)
15. Saito, K., Sakaguchi, Y., Suzuki, T., Siomi, H., and Siomi, M. C. (2007) Pimet, the *Drosophila* homolog of HEN1, mediates 2'-O-methylation of Piwi-interacting RNAs at their 3' ends. *Genes Dev.* **21**, 1603–1608 [CrossRef Medline](#)
16. Kirino, Y., and Mourelatos, Z. (2007) Mouse Piwi-interacting RNAs are 2'-O-methylated at their 3' termini. *Nat. Struct. Mol. Biol.* **14**, 347–348 [CrossRef Medline](#)
17. Horwich, M. D., Li, C., Matranga, C., Vagin, V., Farley, G., Wang, P., and Zamore, P. D. (2007) The *Drosophila* RNA methyltransferase, DmHen1, modifies germline piRNAs and single-stranded siRNAs in RISC. *Curr. Biol.* **17**, 1265–1272 [CrossRef Medline](#)
18. Ohara, T., Sakaguchi, Y., Suzuki, T., Ueda, H., and Miyauchi, K. (2007) The 3' termini of mouse Piwi-interacting RNAs are 2'-O-methylated. *Nat. Struct. Mol. Biol.* **14**, 349–350 [CrossRef Medline](#)
19. Girard, M., Jacquemin, E., Munnich, A., Lyonnet, S., and Henrion-Caude, A. (2008) miR-122, a paradigm for the role of microRNAs in the liver. *J. Hepatol.* **48**, 648–656 [CrossRef Medline](#)
20. Hu, J., Xu, Y., Hao, J., Wang, S., Li, C., and Meng, S. (2012) MiR-122 in hepatic function and liver diseases. *Protein Cell* **3**, 364–371 [CrossRef Medline](#)
21. Sarnow, P., and Sagan, S. M. (2016) Unraveling the mysterious interactions between hepatitis C virus RNA and liver-specific microRNA-122. *Annu. Rev. Virol.* **3**, 309–332 [CrossRef Medline](#)
22. Sarasin-Filipowicz, M., Krol, J., Markiewicz, I., Heim, M. H., and Filipowicz, W. (2009) Decreased levels of microRNA miR-122 in individuals with hepatitis C responding poorly to interferon therapy. *Nat. Med.* **15**, 31–33 [CrossRef Medline](#)
23. Jopling, C. L., Yi, M., Lancaster, A. M., Lemon, S. M., and Sarnow, P. (2005) Modulation of hepatitis C virus RNA abundance by a liver-specific microRNA. *Science* **309**, 1577–1581 [CrossRef Medline](#)
24. Katoh, T., Sakaguchi, Y., Miyauchi, K., Suzuki, T., Kashiwabara, S., and Baba, T. (2009) Selective stabilization of mammalian microRNAs by 3' adenylation mediated by the cytoplasmic poly(A) polymerase GLD-2. *Genes Dev.* **23**, 433–438 [CrossRef Medline](#)
25. Katoh, T., Hojo, H., and Suzuki, T. (2015) Destabilization of microRNAs in human cells by 3' deadenylation mediated by PARN and CUGBP1. *Nucleic Acids Res.* **43**, 7521–7534 [CrossRef Medline](#)
26. D'Ambrogio, A., Gu, W., Udagawa, T., Mello, C. C., and Richter, J. D. (2012) Specific miRNA stabilization by Gld2-catalyzed monoadenylation. *Cell Rep.* **2**, 1537–1545 [CrossRef Medline](#)
27. Burns, D. M., D'Ambrogio, A., Nottrott, S., and Richter, J. D. (2011) CPEB and two poly(A) polymerases control miR-122 stability and p53 mRNA translation. *Nature* **473**, 105–108 [CrossRef Medline](#)
28. Burroughs, A. M., Ando, Y., de Hoon, M. J., Tomaru, Y., Nishibu, T., Ukekawa, R., Funakoshi, T., Kurokawa, T., Suzuki, H., Hayashizaki, Y., and Daub, C. O. (2010) A comprehensive survey of 3' animal miRNA modification events and a possible role for 3' adenylation in modulating miRNA targeting effectiveness. *Genome Res.* **20**, 1398–1410 [CrossRef Medline](#)
29. Kim, G. W., Lee, S. H., Cho, H., Kim, M., Shin, E. C., and Oh, J. W. (2016) Hepatitis C virus core protein promotes miR-122 destabilization by inhibiting GLD-2. *PLoS Pathog.* **12**, e1005714 [CrossRef Medline](#)
30. Wu, J. I., Reed, R. B., Grabowski, P. J., and Artzt, K. (2002) Function of quaking in myelination: regulation of alternative splicing. *Proc. Natl. Acad. Sci. U.S.A.* **99**, 4233–4238 [CrossRef Medline](#)
31. Saccomanno, L., Loushin, C., Jan, E., Punkay, E., Artzt, K., and Goodwin, E. B. (1999) The STAR protein QKI-6 is a translational repressor. *Proc. Natl. Acad. Sci. U.S.A.* **96**, 12605–12610 [CrossRef Medline](#)
32. Larocque, D., Galarneau, A., Liu, H. N., Scott, M., Almazan, G., and Richard, S. (2005) Protection of p27(Kip1) mRNA by quaking RNA binding proteins promotes oligodendrocyte differentiation. *Nat. Neurosci.* **8**, 27–33 [CrossRef Medline](#)
33. Larocque, D., Pilotte, J., Chen, T., Cloutier, F., Massie, B., Pedraza, L., Couture, R., Lasko, P., Almazan, G., and Richard, S. (2002) Nuclear retention of MBP mRNAs in the quaking viable mice. *Neuron* **36**, 815–829 [CrossRef Medline](#)
34. Chénard, C. A., and Richard, S. (2008) New implications for the QUAKE RNA binding protein in human disease. *J. Neurosci. Res.* **86**, 233–242 [CrossRef Medline](#)
35. Aberg, K., Saetre, P., Jareborg, N., and Jazin, E. (2006) Human QKI, a potential regulator of mRNA expression of human oligodendrocyte-related genes involved in schizophrenia. *Proc. Natl. Acad. Sci. U.S.A.* **103**, 7482–7487 [CrossRef Medline](#)
36. Shingu, T., Ho, A. L., Yuan, L., Zhou, X., Dai, C., Zheng, S., Wang, Q., Zhong, Y., Chang, Q., Horner, J. W., Liebelt, B. D., Yao, Y., Hu, B., Chen, Y., Fuller, G. N., et al. (2017) Qki deficiency maintains stemness of glioma stem cells in suboptimal environment by downregulating endolysosomal degradation. *Nat. Genet.* **49**, 75–86 [CrossRef Medline](#)
37. Conn, S. J., Pillman, K. A., Toubia, J., Conn, V. M., Salmanidis, M., Phillips, C. A., Roslan, S., Schreiber, A. W., Gregory, P. A., and Goodall, G. J. (2015) The RNA binding protein quaking regulates formation of circRNAs. *Cell* **160**, 1125–1134 [CrossRef Medline](#)
38. Ebersole, T. A., Chen, Q., Justice, M. J., and Artzt, K. (1996) The quaking gene product necessary in embryogenesis and myelination combines features of RNA binding and signal transduction proteins. *Nat. Genet.* **12**, 260–265 [CrossRef Medline](#)
39. Li, Z. Z., Kondo, T., Murata, T., Ebersole, T. A., Nishi, T., Tada, K., Ushio, Y., Yamamura, K., and Abe, K. (2002) Expression of Hqk encoding a KH RNA binding protein is altered in human glioma. *Jpn. J. Cancer Res.* **93**, 167–177 [CrossRef Medline](#)
40. Li, Z., Zhang, Y., Li, D., and Feng, Y. (2000) Destabilization and mislocalization of myelin basic protein mRNAs in quaking dysmyelination lacking the QKI RNA-binding proteins. *J. Neurosci.* **20**, 4944–4953 [CrossRef Medline](#)
41. Galarneau, A., and Richard, S. (2005) Target RNA motif and target mRNAs of the Quaking STAR protein. *Nat. Struct. Mol. Biol.* **12**, 691–698 [CrossRef Medline](#)
42. Hafner, M., Landthaler, M., Burger, L., Khorshid, M., Hausser, J., Berninger, P., Rothballer, A., Ascano, M., Jr., Jungkamp, A. C., Munschauer, M., Ulrich, A., Wardle, G. S., Dewell, S., Zavolan, M., and Tuschl, T. (2010) Transcriptome-wide identification of RNA-binding protein and microRNA target sites by PAR-CLIP. *Cell* **141**, 129–141 [CrossRef Medline](#)
43. Wang, Y., Lacroix, G., Haines, J., Doukhanine, E., Almazan, G., and Richard, S. (2010) The QKI-6 RNA binding protein localizes with the MBP mRNAs in stress granules of glial cells. *PLoS ONE* **5**, e12824 [CrossRef Medline](#)
44. Akay, A., Craig, A., Lehrbach, N., Larance, M., Pourkarimi, E., Wright, J. E., Lamond, A., Miska, E., and Gartner, A. (2013) RNA-binding protein GLD-1/quaking genetically interacts with the mir-35 and the let-7 miRNA pathways in *Caenorhabditis elegans*. *Open Biol.* **3**, 130151 [CrossRef Medline](#)
45. Yamagishi, R., Tsusaka, T., Mitsunaga, H., Maehata, T., and Hoshino, S. (2016) The STAR protein QKI-7 recruits PAPD4 to regulate post-transcriptional polyadenylation of target mRNAs. *Nucleic Acids Res.* **44**, 2475–2490 [CrossRef Medline](#)
46. Wang, L., Eckmann, C. R., Kadyk, L. C., Wickens, M., and Kimble, J. (2002) A regulatory cytoplasmic poly(A) polymerase in *Caenorhabditis elegans*. *Nature* **419**, 312–316 [CrossRef Medline](#)
47. Nakel, K., Bonneau, F., Eckmann, C. R., and Conti, E. (2015) Structural basis for the activation of the *C. elegans* noncanonical cytoplasmic poly(A)-polymerase GLD-2 by GLD-3. *Proc. Natl. Acad. Sci. U.S.A.* **112**, 8614–8619 [CrossRef Medline](#)

GLD-2 and QKI-7 adenylate and stabilize miRNAs

48. Lee, M., Choi, Y., Kim, K., Jin, H., Lim, J., Nguyen, T. A., Yang, J., Jeong, M., Giraldez, A. J., Yang, H., Patel, D. J., and Kim, V. N. (2014) Adenylation of maternally inherited microRNAs by Wispy. *Mol. Cell* **56**, 696–707 [CrossRef Medline](#)
49. Ren, G., Xie, M., Zhang, S., Vinovskis, C., Chen, X., and Yu, B. (2014) Methylation protects microRNAs from an AGO1-associated activity that uridylylates 5' RNA fragments generated by AGO1 cleavage. *Proc. Natl. Acad. Sci. U.S.A.* **111**, 6365–6370 [CrossRef Medline](#)
50. Wang, Y., Juraneck, S., Li, H., Sheng, G., Wardle, G. S., Tuschl, T., and Patel, D. J. (2009) Nucleation, propagation and cleavage of target RNAs in Ago silencing complexes. *Nature* **461**, 754–761 [CrossRef Medline](#)
51. Yoon, J. H., Jo, M. H., White, E. J., De, S., Hafner, M., Zucconi, B. E., Abdelmohsen, K., Martindale, J. L., Yang, X., Wood W. H 3rd, Shin, Y. M., Song, J. J., Tuschl, T., Becker, K. G., Wilson, G. M., Hohng, S., and Gorospe, M. (2015) AUF1 promotes let-7b loading on Argonaute 2. *Genes Dev.* **29**, 1599–1604 [CrossRef Medline](#)
52. Chen, A. J., Paik, J. H., Zhang, H., Shukla, S. A., Mortensen, R., Hu, J., Ying, H., Hu, B., Hurt, J., Farny, N., Dong, C., Xiao, Y., Wang, Y. A., Silver, P. A., Chin, L., Vasudevan, S., and Depinho, R. A. (2012) STAR RNA-binding protein Quaking suppresses cancer via stabilization of specific miRNA. *Genes Dev.* **26**, 1459–1472 [CrossRef Medline](#)
53. Backes, S., Shapiro, J. S., Sabin, L. R., Pham, A. M., Reyes, I., Moss, B., Cherry, S., and ten Oever, B. R. (2012) Degradation of host microRNAs by poxvirus poly(A) polymerase reveals terminal RNA methylation as a protective antiviral mechanism. *Cell Host Microbe* **12**, 200–210 [CrossRef Medline](#)
54. Boele, J., Persson, H., Shin, J. W., Ishizu, Y., Newie, I. S., Søkilde, R., Hawkins, S. M., Coarfa, C., Ikeda, K., Takayama, K., Horie-Inoue, K., Ando, Y., Burroughs, A. M., Sasaki, C., Suzuki, C., *et al.* (2014) PAPD5-mediated 3' adenylation and subsequent degradation of miR-21 is disrupted in proliferative disease. *Proc. Natl. Acad. Sci. U.S.A.* **111**, 11467–11472 [CrossRef Medline](#)
55. Katoh, T., and Suzuki, T. (2007) Specific residues at every third position of siRNA shape its efficient RNAi activity. *Nucleic Acids Res.* **35**, e27 [CrossRef Medline](#)
56. Zhang, Y., Werling, U., and Edlmann, W. (2012) SLiCE: a novel bacterial cell extract-based DNA cloning method. *Nucleic Acids Res.* **40**, e55 [CrossRef Medline](#)